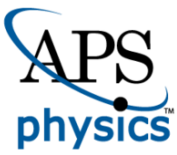

Nanorheology of Entangled Polymer Melts

Ting Ge, Gary S. Grest, and Michael Rubinstein

Phys. Rev. Lett. **120**, 057801 — Published 1 February 2018

DOI: 10.1103/PhysRevLett.120.057801

Nanorheology of Entangled Polymer Melts

Ting Ge,[1] Gary S. Grest,[2] and Michael Rubinstein[1]

[1]*Department of Chemistry, University of North Carolina, Chapel Hill, North Carolina 27599, USA*
[2]*Sandia National Laboratories, Albuquerque, New Mexico 87185, USA*

(Dated: December 6, 2017)

We use molecular simulations to probe local viscoelasticity of an entangled polymer melt by tracking the motion of embedded non-sticky nanoparticles (NPs). As in conventional microrheology, the generalized Stokes-Einstein relation is employed to extract an effective stress relaxation function $G_{GSE}(t)$ from the mean square displacement of NPs. $G_{GSE}(t)$ for different NP diameters d are compared with the stress relaxation function $G(t)$ of a pure polymer melt. The deviation of $G_{GSE}(t)$ from $G(t)$ reflects the incomplete coupling between NPs and the dynamic modes of the melt. For linear polymers, a plateau in $G_{GSE}(t)$ emerges as d exceeds the entanglement mesh size a and approaches the entanglement plateau in $G(t)$ for a pure melt with increasing d. For ring polymers, as d increases towards the spanning size R of ring polymers, $G_{GSE}(t)$ approaches $G(t)$ of ring melt with no entanglement plateau.

Microrheology is a powerful technique to measure the viscoelasticity of a medium through tracking the motion of embedded probe particles[1]. The particles are often much larger than any structural length scale of the medium, and their motion is coupled to the bulk viscoelasticity [2–4]. In this Letter, we use molecular simulations to explore the extension of microrheology to nanorheology, in which nanoparticles (NPs) smaller than or comparable to the structural length scales of the medium are used instead of micron-size beads. Specifically, we study NPs in a melt of entangled polymers. A key question is how viscoelastic modes of the melt affect the NP motion and how it is related to the diameter d of NPs and the structural length scales of the polymer melt, such as the average spacing a between polymer entanglements and the average size R of polymers.

Diffusion of NPs in a polymer melt is an essential process during the fabrication of polymer nanocomposites, a prominent class of hybrid materials [5, 6]. Experiments [7–10] and simulations [6, 11–13] have demonstrated that NP diffusion in a melt of entangled linear polymers depends on the relation between d and a. The mobility of NPs with $d < a$ is higher than the prediction of the Stokes-Einstein relation [12, 13]. Scaling theory [14] argues that these NPs are coupled only to the unentangled dynamics of local chain segments with sizes up to $\approx d$. The mobility of NPs with $d > a$ is suppressed due to the confinement of the entanglement network [12, 13]. While sufficiently large NPs are trapped by the network and cannot freely diffuse until the terminal relaxation of the network, NPs with d moderately larger than a can overcome the entanglement confinement through the hopping diffusion mechanism [15].

Recently, NP diffusion in an entangled melt of non-concatenated ring polymers has also been studied using simulations and scaling theory [13]. The motion of NPs with $d > a$ in ring polymers is not as strongly suppressed as in linear polymers of the same lengths, as there is no entanglement network in a ring polymer melt. The comparison of NP diffusion in entangled linear chains and non-concatenated rings exemplifies the effects of polymer architecture on the dynamical coupling between NPs and polymer melts.

One measure of viscoelasticity is the stress relaxation modulus $G(t)$ as a function of time t. In microrheology, $G(t)$ is linked to the mean squared displacement (MSD) of tracer particles $\langle \Delta r^2(t) \rangle$ through the generalized Stokes-Einstein (GSE) relation [1, 2]. In the domain of Laplace frequency s, the GSE relation is

$$\widetilde{G}(s) = \frac{6k_BT}{f\pi d s \left\langle \widetilde{\Delta r^2}(s) \right\rangle} \tag{1}$$

in which $\widetilde{G}(s)$ and $\widetilde{\Delta r^2}(s)$ are the unilateral Laplace transforms of $G(t)$ and $\langle \Delta r^2(t) \rangle$. $f = 3$ or 2 depending on whether the particle-medium boundaries are stick or slip.

We employ the GSE relation to convert the simulation data of NP MSD in a polymer melt to an effective stress relaxation function $G_{GSE}(t)$. The results of $G_{GSE}(t)$ for NPs with different diameters d are compared with the stress relaxation function of the corresponding pure polymer melt $G_{GK}(t)$, which is obtained using the Green-Kubo formula. This comparison is performed for NPs in entangled linear polymers and non-concatenated ring polymers. Through this comparison, we examine the coupling between NP motion and the bulk melt viscoelasticity and the dependence of the coupling on d.

The models of polymers and NPs are similar to those in previous molecular dynamics (MD) simulations [6, 12, 13, 16–19]. Lennard-Jones units σ, m and ϵ are used for length, mass and energy, respectively. For the entangled linear polymer melt, the number of monomers per entanglement strand $N_e \approx 28$ [20, 21], the average spacing between entanglements $a \approx 5\sigma$ [21], and the entanglement time $\tau_e \approx 4000\tau$ [22] with $\tau = \sigma\sqrt{m/\epsilon}$. The number of monomers in a polymer is $N = 800$ for both linear chains and rings. NP diameter d ranges from

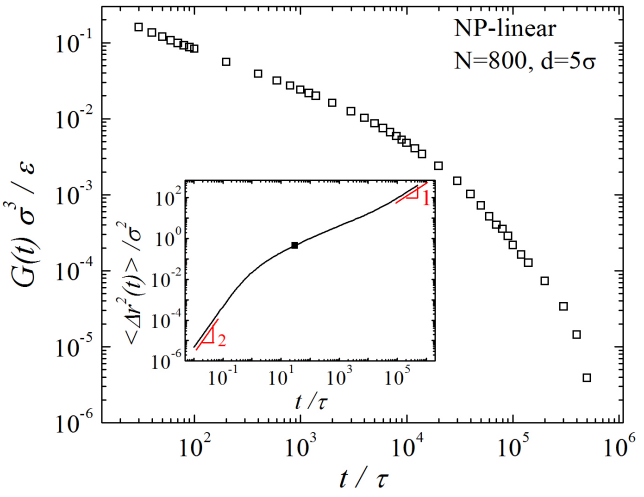

FIG. 1. $G_{GSE}(t)$ (open squares) for $d = 5\sigma$ in linear polymers with $N = 800$. The corresponding $\langle \Delta r^2(t) \rangle$ is shown in the inset (see black line). The log-log slope $\alpha = 2$ for the ballistic regime and $\alpha = 1$ for the Fickian regime are indicated. The estimated end of the crossover between ballistic and thermal motion is indicated by the black square.

$3\sigma < a$ to $15\sigma \approx 3a$, and the volume fraction of NPs $\phi_{NP} \approx 10\%$. Previous simulations [6] have shown that the viscosity of a NP linear polymer composite is reduced with respected to that of the corresponding pure polymer melt if $d < a$, almost unchanged if $d \approx a$, while enhanced if $d > a$. The relative change of composite viscosity with respect to pure melt viscosity can be up to $\approx 25\%$ at $\phi_{NP} \approx 10\%$. For NP-ring systems, our simulation results show that the composite viscosity at $\phi_{NP} \approx 10\%$ also changes by up to $\approx 25\%$ depending on d. All samples were equilibrated at pressure $P = 0$ and temperature $T = 1.0\epsilon/k_B$. Subsequent simulations were run at constant volume V for up to $10^8\tau$. MSDs $\langle \Delta r^2(t) \rangle$ of NPs in the simulations have been reported in a previous paper [13]. Additional simulation details are presented in Supplemental Material (SM).

The stress relaxation modulus for a pure polymer melt is calculated using the Green-Kubo formula

$$G^{ij}_{GK}(t) = \frac{V}{k_B T} \left\langle \overline{\sigma^{ij}}(t) \overline{\sigma^{ij}}(0) \right\rangle \qquad (2)$$

where $\overline{\sigma^{ij}}(t)$ is the pre-averaged stress [23], and i and j are Cartesian indices with $i \neq j$. $G_{GK}(t)$ is computed as the average of $G^{ij}_{GK}(t)$ with $ij = xy$, xz and yz.

We use the GSE relation (Eq. 1) to convert $\langle \Delta r^2(t) \rangle$ to $G_{GSE}(t)$. The conversion is done using the method developed by Mason [24]. One example of the conversion is given in Fig. 1. The early-time part of $\langle \Delta r^2(t) \rangle$ is excluded from the conversion, as the inertialess GSE relation (Eq. 1) is not applicable to the regime of ballistic motion and the subsequent crossover to thermal motion [25]. As shown in the inset of Fig. 1, a typical MSD curve starts with a ballistic regime where the log-log slope $\alpha = d \log \langle \Delta r^2(t) \rangle / d \log t = 2$, then it crosses over to a sub-diffusive regime with $\alpha < 1$, and eventually enters the Fickian regime with $\alpha = 1$. We estimate that the crossover from ballistic to thermal motion ends at the inflection point of α vs. $\log t$. The black square in the inset of Fig. 1 indicates the end of the crossover at $\tau^* \approx 30\tau$ for $d = 5\sigma$. A detailed discussion of this criterion for τ^* can be found in SM. Only $\langle \Delta r^2(t) \rangle$ for $t > \tau^*$ is used in the conversion to $G_{GSE}(t)$.

Throughout the paper, we use $f = 2$ for the GSE relation, which corresponds to slip NP-polymer boundaries. The slip boundary results from the slip length $L_s(t)$ being larger than d for $t > \tau^*$. Previous simulations [26] have demonstrated that L_s for a bulk polymer melt scales linearly with the melt viscosity η. To estimate $L_s(t)$ in the present simulations, a similar scaling relation $L_s(t) \approx b\,[\eta(t)/\eta_0]$, in which monomer size $b \approx \sigma$ and monomeric viscosity $\eta_0 \approx \tau k_B T/\sigma^3$, is used. In SM, we estimate $\eta(t)$ from $\int_0^t G_{GK}(t')dt'$ and demonstrate that the condition $L_s(t) > L_s(\tau^*) > d$ for $t > \tau^*$ is satisfied in all simulated NP-polymer systems (see Fig. S1), justifying the slip NP-polymer boundaries.

Results of $G_{GK}(t)$ and $G_{GSE}(t)$ for linear polymers are shown in Fig. 2(a). For $G_{GK}(t)$, there is first a power-law decay, then the development of entanglement plateau, and finally the regime of terminal relaxation. At $t \approx 6.5 \times 10^4\tau$ with the smallest log-log slope $|-d \log G(t)/d \log t| \approx 0.07$, $G(t) \approx 2.6 \times 10^{-2}\epsilon/\sigma^3$, which is close to the theoretical prediction [27] of the entanglement plateau $G_e \approx 4\rho k_B T/5N_e \approx 2.5 \times 10^{-2}\epsilon/\sigma^3$ with melt density $\rho = 0.89\sigma^{-3}$ and $N_e \approx 28$. The power-law decrease can be described using the Rouse modes of short unentangled sections of polymer, and is predicted to scale as $G(t) \sim t^{-1/2}$ [28]. The entanglement plateau has been successfully understood based on the phenomenological tube model [27, 28], in which entangled chains are confined in their respective tubes with average diameter $\approx a$. For $Z = N/N_e \approx 30$ as in the present simulations, dynamic processes such as Rouse-type relaxation along the tube, tube length fluctuation and constraint release contribute to the partial stress relaxation prior to the terminal relaxation [29], and results in the deviation of the plateau from a horizontal line. To compare the simulation data of $G_{GK}(t)$ with theories for polymer stress relaxation, we fit $G_{GK}(t)$ to the theoretical expression proposed by Likhtman and McLeish [29]. The details of the fitting are presented in SM. The parameters of the best fit are $N/N_e = Z = 33 \pm 1$, $N_e = 24 \pm 1$, $\tau_e = (1.9 \pm 0.1) \times 10^3\tau$, and $G_e = (0.030 \pm 0.002)\,\epsilon/\sigma^3$.

The melt viscoelasticity that affects the thermal NP motion in linear chains depends on d, as demonstrated in the d-dependence of $G_{GSE}(t)$ in Fig. 2(a). For $d = 3\sigma < a$ and $d = 5\sigma \approx a$, there is no plateau in $G_{GSE}(t)$. The dynamic modes of local chain segments that control the motion of NPs with $d \leq a$ contribute to $G_{GSE}(t)$.

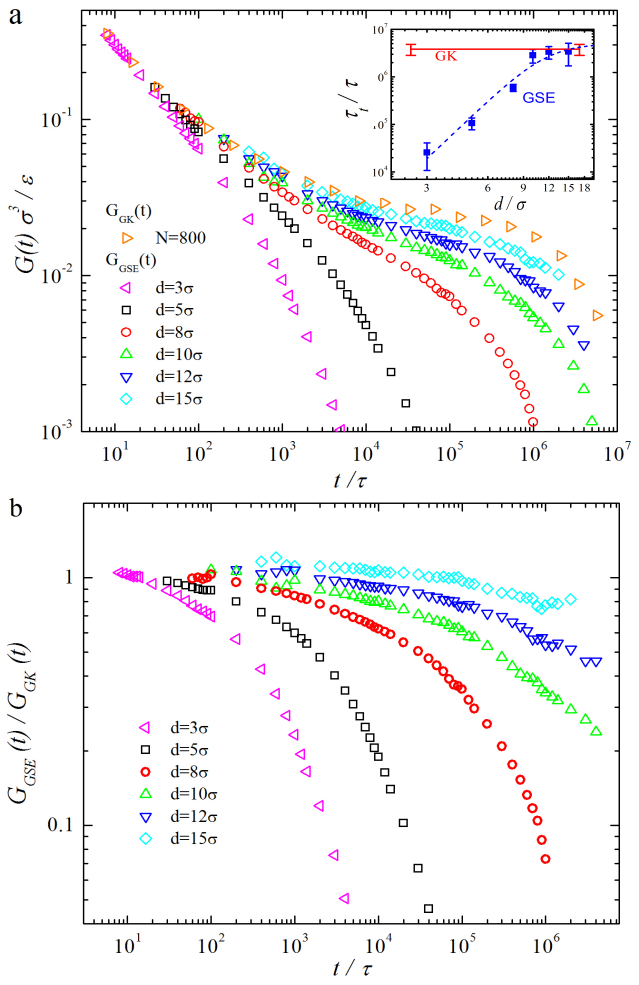

FIG. 2. (a) $G_{GSE}(t)$ for NPs with different d in linear polymers with $N = 800$ compared to $G_{GK}(t)$ for the pure linear polymer melt. Inset shows τ_t vs. d for $G_{GSE}(t)$ (blue squares) and τ_t for $G_{GK}(t)$ (red line) with error bars. The dashed blue line indicates the best fit to the scaling theory prediction [15]. (b) The ratio $G_{GSE}(t)/G_{GK}(t)$ for the same systems as in (a).

The degree of coupling between NP motion and these dynamic modes is quantified by the ratio $G_{GSE}(t)/G_{GK}(t)$ (see Fig. 2(b)). As t increases, $G_{GSE}(t)/G_{GK}(t)$ drops below 1, indicating reduced degree of coupling between NP motion and the corresponding dynamic modes. The decrease of $G_{GSE}(t)/G_{GK}(t)$ is less rapid for $d = 5\sigma$ than for $d = 3\sigma$, indicating stronger coupling between NP motion and the melt viscoelasticity with increasing d. Scaling theory [14] predicts that the motion of a NP with $d < a$ is coupled to the Rouse modes of chain segments with sizes up to d. Motivated by the theory, we compare $G_{GSE}(t)$ for $d \le a$ with

$$G(t) = \frac{\rho k_B T}{N} \sum_{p=p_c}^{N} \exp\left(-\frac{2tp^2}{\tau_R}\right) \qquad (3)$$

which is the sum of the modes with Rouse time τ_R and mode indices $p_c \le p \le N$. $N = 800$ and N/p_c is the number of monomers in the largest chain segment that affects NP motion. The comparison is presented in SM.

As d exceeds a, a plateau regime emerges as indicated by the inflection in the log-log plot of $G_{GSE}(t)$. The presence of a plateau means that NPs with $d > a$ are affected by the confinement of the entanglement network. The confinement is stronger for larger d, and the coupling between NP motion and melt viscoelasticity is enhanced with increasing d, as shown in Fig. 2(b). However, for the largest $d = 15\sigma$, the coupling is still not complete with $G_{GSE}(t)/G_{GK}(t) < 1$. We fit $G_{GSE}(t)$ for $d > a$ to the Likhtman-McLeish expression [29] (eq. S1). As shown in SM, the best-fit value of the number of entanglements per chain Z increases with d, but stays below $Z = 33$ for the bulk melt. The reason of the partial coupling for $8\sigma \le d \le 15\sigma$ has been attributed to the hopping diffusion [13, 15] for d moderately larger than a.

The terminal regime of $G(t)$ in Fig. 2(a) is fit to an exponential decay with $G(t) \sim \exp(-t/\tau_t)$, where τ_t is the characteristic decay time. While τ_t characterizes terminal stress relaxation in the pure melt, τ_t for $G_{GSE}(t)$ is essentially the terminal diffusion time of NP motion. The results of τ_t for $G_{GSE}(t)$ and $G_{GK}(t)$ are shown in the inset of Fig. 2(a). τ_t for $G_{GSE}(t)$ increases with d and then saturates around τ_t for $G_{GK}(t)$ as d exceeds 10σ. Despite the saturation of τ_t, $G_{GSE}(t)$ is still below $G_{GK}(t)$ for $d \ge 10\sigma$. This suggests that NPs with $d \ge 10\sigma$ are coupled to the melt dynamics up to the longest terminal relaxation mode, though the coupling is not complete. Scaling theory [15] predicts that $\tau_t \sim d^4$ for $d < a$, $\tau_t \sim \exp(d/a)$ for hopping diffusion, and finally τ_t saturates at the terminal relaxation time of the melt in the large d limit. The best fit of the d-dependence of τ_t to an analytical function motivated by the theory is shown by the dashed line in the inset of Fig. 2a. Details about the fitting and the terminal regimes are in SM.

Results of $G_{GK}(t)$ and $G_{GSE}(t)$ for ring polymers are shown in Fig. 3. Unlike $G_{GK}(t)$ for linear polymers, $G_{GK}(t)$ for ring polymers has no entanglement plateau, as there is no long-lived entanglement network [30]. The melt viscoelasticity that determines the diffusion of NPs in rings depends on d, as demonstrated by the d-dependence of $G_{GSE}(t)$ in Fig. 3. As d increases, $G_{GSE}(t)$ for NPs in rings approaches $G_{GK}(t)$ for pure rings, and the ratio $G_{GSE}(t)/G_{GK}(t)$ deviates from 1 less rapidly with increasing t (see the inset of Fig. 3). These results show that NP motion is coupled to the melt viscoelasticity over a wider spectrum of relaxation modes with increasing d, and the coupling is stronger for larger d. Scaling theory [13] predicts that NP motion is coupled to the dynamics of ring sections with sizes up to d, which is smaller than the size of an entire ring polymer.

The motion of NPs with sufficiently large d is expected to be completely coupled to the terminal relaxation of the

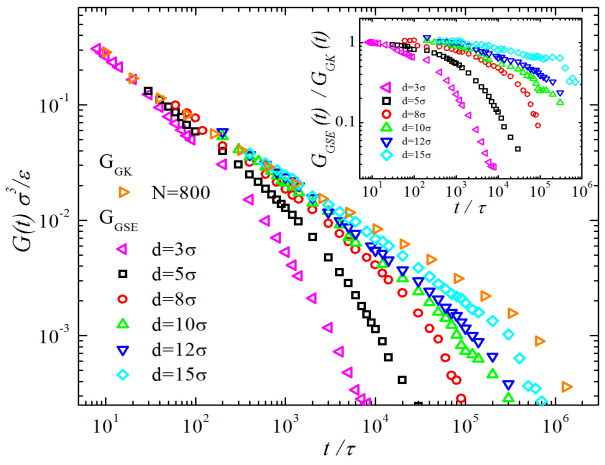

FIG. 3. $G_{GSE}(t)$ for NPs with different d in ring polymers with $N = 800$ compared to $G_{GK}(t)$ for the pure linear polymer melt. Inset shows the ratio $G_{GSE}(t)/G_{GK}(t)$.

polymer melt, and the corresponding $G_{GSE}(t)$ excluding the early-time part affected by NP inertia is expected to agree with $G_{GK}(t)$. Previously, based on the examination of the d-dependence of the diffusion coefficient D for the same simulations [13], it is estimated that the Stokes-Einstein (SE) relation $D = k_BT/2\pi\eta d$, where η is the melt viscosity, is recovered for $d > d_c \approx 20\sigma$ in NP-linear systems ($N = 800$), and for $d > d_c \approx 30\sigma$ in NP-ring systems ($N = 800$). Since the recovery of SE relation corresponds to a complete coupling between Fickian NP motion and the melt viscoelasticity, we expect that the threshold NP size d_c for the agreement between $G_{GSE}(t)$ and $G_{GK}(t)$ is also 20σ and 30σ for NP-linear and NP-ring systems ($N = 800$), respectively.

The important length scale that determines the agreement between $G_{GSE}(t)$ and $G_{GK}(t)$ differs for NPs in linear and ring polymers. d is compared with the entanglement spacing a to determine whether $G_{GSE}(t)$ and $G_{GK}(t)$ agrees for NPs in linear chains. According to the hopping diffusion model [15], the hopping probability decreases as $\sim \exp(-d/a)$. Hopping diffusion is suppressed for d sufficiently larger than a, and therefore the NP motion is completely coupled to the relaxation of the entanglement network even for d smaller than the size of linear chains. In the present simulation, the estimated $d_c \approx 4a$ for the complete coupling between NPs and linear polymers. By contrast, d is compared with the average spanning size $\langle R^2 \rangle^{1/2}$ of ring polymers to determine the agreement between $G_{GSE}(t)$ and $G_{GK}(t)$. As there is no long-lived entanglement network to confine NPs in ring polymers, NP motion is increasingly coupled to ring dynamics at longer time scales and larger length scales as d increases towards $\langle R^2 \rangle^{1/2}$. In the present simulations, $\langle R^2 \rangle^{1/2} \approx 15\sigma$, and the estimated $d_c \approx 2\langle R^2 \rangle^{1/2}$ for the coupling between NPs and the entire relaxation dynamics of rings. $d_c \approx 2\langle R^2 \rangle^{1/2}$ results from the broad distribution of R around the average $\langle R^2 \rangle^{1/2}$. Our analysis in SM shows that 33% of all R are larger than $\langle R^2 \rangle^{1/2}$, while almost all (99%) R are smaller than $d = 2\langle R^2 \rangle^{1/2}$. This explains why NPs with $d = 15\sigma$ are not completely coupled to the entire ring dynamics, whereas NPs with $d > 2\langle R^2 \rangle^{1/2}$ are anticipated to be almost completely coupled.

Another important length scale for NP-polymer coupling is the slip length L_s at NP-polymer boundaries. Present simulations correspond to slip boundary condition with $L_s > d$. If $d > L_s$, the boundary condition becomes stick. There would be a scaling regime where NP motion is fully coupled to all relaxation modes of polymers but with stick NP-polymer boundaries. Fig. S9 shows the scaling theory prediction for such a regime depending on d and polymer size. The existence of two length scales d_c and L_s suggests a two-stage coupling of NPs to entire polymer dynamics with increasing d. NPs are first coupled to all relaxation modes with slip NP-polymer boundaries as d exceeds d_c. Subsequently, the boundary conditions change from slip to stick as d further increases above L_s.

To summarize, on the basis of molecular simulations, we compare the stress relaxation moduli $G_{GSE}(t)$ converted from NP MSD through the generalized Stokes-Einstein relation and $G_{GK}(t)$ for pure entangled polymer melts calculated using the Green-Kubo formula. The deviation of $G_{GSE}(t)$ from $G_{GK}(t)$ results from the incomplete coupling of NP motion to the relaxation modes of polymer melt. The threshold NP size d_c for the agreement between $G_{GSE}(t)$ and $G_{GK}(t)$ is compared to the entanglement mesh size for NP-linear systems whereas to the polymer size for NP-ring systems in which there are no entanglement networks. Our simulations correspond to slip NP-polymer boundaries, but a change from slip to stick boundaries as d increases above the slip length L_s is anticipated. NP-polymer coupling with increasing d is proposed to be a two-stage process depending on d_c and L_s. Our study should help extend the well-established micro-rheology procedures to nanorheology, which would advance the study of local viscoelasticity that controls the dynamics of nano-scale objects in a viscoelastic medium, such as NPs in polymer nanocomposites and NP-based drug carriers in living cells.

M. R. acknowledges financial support from the National Science Foundation under Grants DMR-1309892, DMR-1436201, and DMR-1121107, the National Institutes of Health under Grants P01-HL108808 and 1UH2HL123645, and the Cystic Fibrosis Foundation. This research used resources at the National Energy Research Scientific Computing Center, which is supported by the Office of Science of the United States Department of Energy under Contract No. DE-AC02-05CH11231.

This work was performed, in part, at the Center for Integrated Nanotechnologies, an Office of Science User Facility operated for the U.S. Department of Energy (DOE) Office of Science. Sandia National Laboratories is a multimission laboratory managed and operated by National Technology and Engineering Solutions of Sandia, LLC., a wholly owned subsidiary of Honeywell International, Inc., for the U.S. Department of Energys National Nuclear Security Administration under contract DE-NA-0003525.

[1] T. M. Squires and T. G. Mason, Annu. Rev. Fluid Mech. **42**, 413 (2010).
[2] T. G. Mason and D. A. Weitz, Phys. Rev. Lett. **74**, 1250 (1995).
[3] B. R. Dasgupta, S. Y. Tee, J. C. Crocker, B. J. Frisken, and D. A. Weitz, Phys. Rev. E **65**, 051505 (2002).
[4] J. H. van Zanten, S. Amin, and A. A. Abdala, Macromolecules **37**, 3874 (2004).
[5] A. C. Balazs, T. Emrick, and T. P. Russell, Science **314**, 1107 (2006).
[6] J. T. Kalathi, G. S. Grest, and S. K. Kumar, Phys. Rev. Lett. **109**, 198301 (2012).
[7] J. Szymanski, A. Patkowski, A. Wilk, P. Garstecki, and R. Holyst, J. Phys. Chem. B **110**, 25593 (2006).
[8] H. Guo, G. Bourret, R. B. Lennox, M. Sutton, J. L. Harden, and R. L. Leheny, Phys. Rev. Lett. **109**, 055901 (2012).
[9] C. A. Grabowski and A. Mukhopadhyay, Macromolecules **47**, 7238 (2014).
[10] R. Mangal, S. Srivastava, S. Narayanan, and L. A. Archer, Macromolecules **32**, 596 (2016).
[11] J. Liu, D. Cao, and L. Zhang, J. Phys. Chem. **112**, 6653 (2008).
[12] J. T. Kalathi, U. Yamamoto, K. S. Schweizer, G. S. Grest, and S. K. Kumar, Phys. Rev. Lett. **112**, 108301 (2014).
[13] T. Ge, J. T. Kalathi, J. D. Halverson, G. S. Grest, and M. Rubinstein, Macromolecules **50**, 1749 (2017).
[14] L. H. Cai, S. Panyukov, and M. Rubinstein, Macromolecules **44**, 7853 (2011).
[15] L. H. Cai, S. Panyukov, and M. Rubinstein, Macromolecules **48**, 847 (2014).
[16] J. D. Halverson, W. B. Lee, G. S. Grest, Y. A. Grosberg, and K. Kremer, J. Chem. Phys. **134**, 204904 (2011).
[17] J. D. Halverson, W. B. Lee, G. S. Grest, Y. A. Grosberg, and K. Kremer, J. Chem. Phys. **134**, 204905 (2011).
[18] K. Kremer and G. S. Grest, J. Chem. Phys. **92**, 5057 (1990).
[19] P. J. in't Veld, S. J. Plimpton, and G. S. Grest, Comput. Phys. Commun. **179**, 320 (2008).
[20] R. Everaers, S. K. Sukumaran, G. S. Grest, C. Svaneborg, A. Sivasubramanian, and K. Kremer, Science **303**, 823 (2004).
[21] H.-P. Hsu and K. Kremer, J. Chem. Phys. **144**, 154907 (2016).
[22] T. Ge, M. O. Robbins, D. Perahia, and G. S. Grest, Phys. Rev. E. **90**, 012602 (2014).
[23] W. B. Lee and K. Kremer, Macromolecules **42**, 6270 (2009).
[24] T. G. Mason, Rheol Acta **39**, 371 (2000).
[25] The effects of the inertia of both probe particle and viscoelastic medium on particle-based passive rheology have been examined in recent theoretical [31] and computational [32, 33] work.
[26] N. V. Priezjev and S. M. Troian, Phys. Rev. Lett. **92**, 018302 (2004).
[27] M. Doi and S. F. Edwards, *The Theory of Polymer Dynamics* (Clarendon Press, Oxford, 1986).
[28] M. Rubinstein and R. H. Colby, *Polymer Physics* (Oxford, 2003).
[29] A. E. Likhtman and T. C. B. McLeish, Macromolecules **35**, 6332 (2002).
[30] M. Kapnistos, M. Lang, D. Vlassopoulos, W. Pyckhout-Hintzen, D. Richter, D. Cho, T. Chang, and M. Rubinstein, Nat. Mater. **7**, 997 (2008).
[31] T. Indei, J. D. Schieber, A. Córdoba, and E. Pilyugina, Phys. Rev. E **85**, 021504 (2012).
[32] M. Karim, S. C. Kohale, T. Indei, J. D. Schieber, and R. Khare, Phys. Rev. E **86**, 051501 (2012).
[33] M. Karim, T. Indei, J. D. Schieber, and R. Khare, Phys. Rev. E **93**, 012501 (2016).